Cognitive Computation (2025) 17:90
https://doi.org/10.1007/s12559-025-10447-9

RESEARCH

Investigating Brain Lobe Biomarkers to Enhance Dementia Detection Using EEG Data

Siuly Siuly[1,2] · Md.Nurul Ahad Tawhid[3,4] · Yan Li[4] · Rajendra Acharya[4] · Muhammad Tariq Sadiq[5] · Hua Wang[1]

Received: 1 October 2024 / Accepted: 18 March 2025 / Published online: 2 April 2025

Abstract

Dementia is a growing global health concern that significantly impacts the quality of life for millions of individuals and imposes substantial burdens on healthcare systems. Early detection and accurate diagnosis are crucial for effective dementia management. Electroencephalography (EEG) has emerged as a non-invasive tool for identifying dementia-related abnormalities and assessing brain function. However, existing EEG-based methods often fail to pinpoint specific biomarkers, particularly brain lobe changes. Brain lobe analysis in EEG is essential for advancing dementia detection and improving diagnostic accuracy. This study aims to address this gap by exploring key brain lobes involved in dementia detection and classification, focusing on Alzheimer's disease (AD) and Frontotemporal dementia (FTD). We introduce a Short-Time Fourier Transform to generate spectrogram images from EEG signals combined with Convolutional Neural Networks to identify the most critical brain lobes for enhanced dementia detection. We have applied Grad-CAM method to improve result interpretability and offer meaningful insights to the research community. Our experiments on OpenNeuro ds004504 EEG dataset for AD and FTD indicate that the parietal lobe exhibits the most significant changes in both conditions, achieving 95.72% accuracy for FTD and 92.25% for AD, followed by the temporal and frontal lobes. When applying the proposed framework to the entire brain region, we achieved 95.59% accuracy for AD and 93.14% for FTD. The findings from EEG-based brain lobe analysis aid experts in improving diagnostic and monitoring tools for neurodegenerative disorders, thereby advancing the understanding and clinical management of dementias like AD and FTD.

Keywords Electroencephalogram · Dementia · Alzheimer's disease · Frontotemporal dementia · EEG signal processing · Short-time fourier transform · Convolutional neural networks

Introduction

Dementia is a group of neurodegenerative disorders characterized by cognitive impairment, memory loss, and difficulties in daily activities due to the progressive degeneration of brain cells. People living with face numerous challenges, including functional limitations, social isolation, emotional distress, health complications, and financial strain. It is the second leading cause of death in Australia and ranks seventh globally [1]. The social and economic impacts of dementia are profound, as it places immense strain on individuals, families, communities, and healthcare systems. According to the World Health Organization (WHO), over 55 million people currently live with dementia, with cases projected to rise to 78 million by 2030 and 139 million by 2050 [2, 3]. This growing prevalence places a significant burden on healthcare systems and economies, with global dementia-related

✉ Siuly Siuly
siuly.siuly@vu.edu.au

✉ Md.Nurul Ahad Tawhid
tawhid@iit.du.ac.bd

1 Institute for Sustainable Industries & Liveable Cities, Victoria University, Melbourne, Australia

2 Centre for Health Research, University of Southern Queensland, Toowoomba, Australia

3 Institute of Information Technology, University of Dhaka, Dhaka, Bangladesh

4 School of Mathematics, Physics and Computing, University of Southern Queensland, Toowoomba, Australia

5 School of Computer Science and Electronic Engineering, University of Essex, Colchester, UK

costs reaching $1.3 trillion USD in 2019, half of which was attributed to informal caregiving [2].

Dementia includes several types, such as Alzheimer's disease (AD), frontotemporal dementia (FTD), vascular dementia (VaD), and dementia with Lewy bodies (DLB). AD is the most common form, accounting for 60–70% of cases [4]. Mild cognitive impairment (MCI) is often considered a precursor to dementia, with an increased risk of progression, though the rate varies among individuals. This study focuses on two of the most common forms of dementia-AD and FTD, which share overlapping symptoms, making accurate diagnosis and targeted treatment development particularly challenging.

Despite its devastating impact, dementia has no cure or treatment to halt or reverse its progression. However, early detection can help mitigate its effects and improve patients' quality of life. Traditional diagnostic methods for dementia, such as clinical assessments and neuroimaging techniques (MRI, PET scans), are expensive, time-consuming, and not widely accessible. As a result, researchers are increasingly exploring non-invasive, cost-effective alternatives, such as electroencephalography (EEG). EEG is a promising tool for studying brain activity due to its high temporal resolution, affordability, and ease of use. EEG captures the electrical activity of the brain through electrodes placed on the scalp, allowing researchers to analyze patterns of neural oscillations and connectivity [5]. Dementia-related changes in brain function can be reflected in EEG signals, particularly in different brain lobes responsible for cognition, memory, and sensory processing.

The human brain consists of several lobes-frontal, temporal, parietal, and occipital—each playing a crucial role in cognitive processing. Studies have linked EEG abnormalities in specific lobes to dementia-related neurodegeneration. For example, temporal lobe disruptions are commonly associated with memory and language deficits in AD, while frontal and parietal lobe alterations may indicate cognitive impairment and executive dysfunction [4]. Recent research suggests that identifying lobe-specific EEG biomarkers can enhance dementia detection accuracy.

This study aims to investigate brain lobe biomarkers derived from EEG data to enhance dementia detection. By focusing on lobe-specific EEG alterations, we seek to improve diagnostic accuracy and contribute to the development of non-invasive, accessible, and reliable tools for early dementia detection.

Existing Work/Prior Art

In recent years, numerous studies have focused on detecting various types of dementia using EEG signals [6–29]. These studies have employed a range of machine learning (ML) algorithms combined with different feature extraction techniques for EEG-based dementia detection. Feature extraction methods such as time, frequency, and time–frequency analysis [6–10, 19], entropy measures [11, 16], connectivity measures [12, 13], complexity measures [14], and event-related analysis [15] have been used in conjunction with well-established ML models, including support vector machines (SVM) [8, 9, 12, 13, 18, 19], *k*-nearest neighbors (kNN) [8, 11, 12, 16], logistic regression [15], random forests [16], and neural networks [10].

Traditional machine learning methods, which typically rely on shallow architectures with at most one layer of nonlinear feature transformation, have limitations in effectively capturing the complex patterns hidden in EEG signals. As a result, these models may fail to detect the deeper characteristics of AD and related dementias. To address this challenge, deep learning (DL) methodologies have become increasingly popular because of their ability to automatically extract and learn features directly from raw EEG data. This approach eliminates the need for hand-crafted features or prior domain-specific knowledge, making the feature extraction process more efficient and data-driven.

In their 2023 study, Alvi et al. [20] introduced a deep learning framework utilizing a Long Short-Term Memory (LSTM) model. Their approach successfully differentiates individuals with MCI, an early stage of AD, from healthy controls. That same year, Ravikanti and Saravanan [21] proposed an Optimized Transformer-based Attention Long Short-Term Memory (OTA-LSTM) model designed for AD detection using EEG signals. In [22], Chaabene et al. differentiated amnestic MCI (aMCI), non-amnestic MCI (naMCI), and healthy controls (HC) during a verbal fluency task (VFT) using EEG data. A transformer-based MCI detection method is proposed, achieving up to 94.78% accuracy. In 2024, Siuly et al. [5] employed LSTM to discern the most effective EEG rhythms and channels for diagnosing AD. Tawhid et al. [23] introduced a Convolutional Neural Network (CNN)-based framework to pinpoint precise frequency band biomarkers for MCI diagnosis. Hasoon et al. [24] explored EEG functional connectivity to differentiate stable MCI from converting MCI. Patients who progress to dementia show altered EEG connectivity in alpha and beta bands, making these measures valuable for early prediction. Şeker and Özerdem [25] investigated spectral and synchrony neuromarkers from resting-state EEG for MCI detection, identifying peak amplitudes and weighted Phase Lag Index (wPLI) in high-frequency bands as effective biomarkers. Adebisi et al. [26] employed Phase Lag Index (PLI) and Graph Convolution Network (GCN-net) on EEG-based brain functional networks (BFNs), achieving 95.07% accuracy (delta) and 80.62% (theta) in distinguishing MCI, AD, and vascular dementia (VD). Sen et al. [27] introduced an intrinsic time-scale decomposition (ITD)-based EEG method for AD detection, achieving 94% accuracy in Q1,

surpassing raw EEG (88.40% in Q2). In 2025, Şeker and Özerdem [28] explored MCI classification using EEG data, transforming raw signals into input images for deep learning. CNNs, transfer learning, hybrid models, and Vision Transformer (ViT) achieve effective classification. Acharya et al. [29] proposed EEGConvNeXt, a lightweight 2D CNN model that converts EEG signals into power spectrogram images for classifying AD, FD, and controls. It features a transformer-based CNN structure with stem, main model, downsampling, and output stages.

Motivation, Problem Description, and Objectives

Detecting dementia using EEG signals is challenging due to the complex and dynamic nature of brain activity, which complicates the extraction of meaningful features to differentiate between healthy individuals and those with dementia. The recent literature reveals a gap in research regarding which brain lobes are most effective as biomarkers for the efficient diagnosis of dementia, such as AD and FTD, using EEG data. Identifying the specific brain regions or lobes that provide critical information for dementia detection is crucial, as these biomarkers are essential for understanding the brain activity patterns associated with the disease. The key aim of this study is to address this gap by developing a deep learning-based model that utilizes spectrogram images and CNN to identify the most effective brain lobes for improved dementia detection.

Our Method

This study proposes a novel framework combining short-time Fourier transform (STFT) and CNN to identify key brain lobes as biomarkers for detecting dementia, specifically AD and FTD, using EEG data. The framework begins by preprocessing the EEG signals, where noise is removed using a butterworth band-pass filter, automatic artifact rejection, and independent component analysis (ICA). The EEG signals are then segmented into smaller time frames. Next, the EEG channels are organized into five brain lobes based on biological principles. Spectrogram images are generated for each brain lobe and the full set of EEG channels using STFT, which provides a time–frequency representation of brain activity. These spectrograms are subsequently fed into a deep learning-based CNN, which is trained to classify dementia. The classification is performed independently on the spectrogram images from each brain lobe as well as from the full channel set.

The combination of STFT and CNN is particularly effective for dementia detection because STFT captures both the time and frequency domains of the brain's electrical activity, offering insights into cognitive decline. CNNs, known for their ability to detect patterns in 2D data such as spectrograms, are adept at learning complex and subtle features associated with dementia. By leveraging the strengths of both techniques, this approach aims to detect dementia-related abnormalities in brain wave patterns more effectively.

Novelties and Contributions

To our knowledge, no research has explored which brain lobes are most responsive in providing critical information for effective dementia detection. This study offers several significant contributions:

- *Novel framework development*: It introduces a new framework for dementia detection that integrates STFT with CNN algorithms, capable of distinguishing between AD, FTD, and HC using EEG data.
- *Innovative approach*: This study is the first to use STFT-based spectrogram images alongside a CNN model for detecting dementia.
- *Brain lobe analysis*: It investigates which brain lobes are most crucial for extracting representative information for effective dementia detection.
- *Performance enhancement*: The study aims to improve the performance of dementia detection compared to existing methods.

Remainder of the Article

The remainder of this paper is structured as follows: the "Proposed Methodology Framework" section outlines the data analyzed and the proposed methodology. The "Experiments and Results" section presents the experimental setup and results, while the "Discussion" section discusses the experimental results and overall findings. Finally, the "Conclusions and Future Plan" section concludes the paper and discusses future work.

Proposed Methodology Framework

In this study, we propose a framework for identifying key brain lobes for detecting dementia including AD and FTD using EEG brain signal data. An overview of the proposed framework is illustrated in Fig. 1, with detailed descriptions provided in the following subsections.

Dataset Description

In our study, we used a publicly available EEG dataset: OpenNeuro ds004504 [8, 30, 31]. This dataset comprises EEG recordings from 88 participants at the Department of Neurology, AHEPA General University Hospital of Thessaloniki. The participants were categorized into three groups:

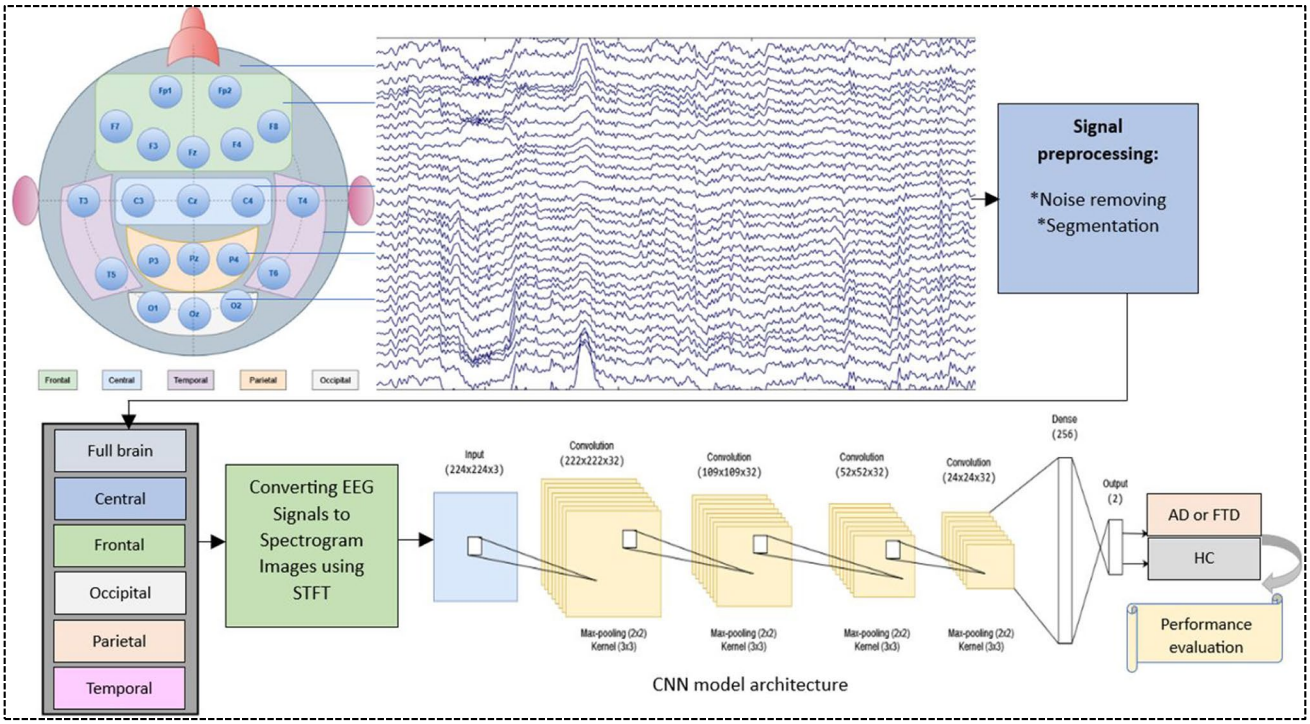

Fig. 1 Overview of the proposed framework for detecting dementia using EEG brain signal data

- Alzheimer's disease (AD): This group consisted of 36 participants (13 males, 23 females) with an average age of 66.4 ± 7.9 years. Their cognitive status was assessed using the Mini-Mental State Examination (MMSE), where lower scores indicated greater cognitive decline. The average MMSE score for this group was 17.75.
- Frontotemporal dementia (FTD): The FTD group included 23 participants (14 males, 9 females) with an average age of 63.6 ± 8.2 years. Their average MMSE score was 22.17.
- Healthy controls (HC): The CN group comprised 29 participants (11 males, 18 females) with a mean age of 67.9 ± 5.4 years. Remarkably, their MMSE scores were perfect, achieving a score of 30.

The EEG data was recorded from 19 electrode channels (Fz, F3, F4, F7, F8, Fp1, Fp2, T3, T4, T5, T6, Cz, C3, C4, Pz, P3, P4, O1, and O2) following the 10–20 international system. Two reference electrodes (A1 and A2) were used. During the eye-closed resting state, EEG data was sampled at a frequency of 500 Hz. Recording durations varied approximately 13.5 min (range: 5.1 to 21.3 min) for AD group, 12 min (range: 7.9 to 16.9 min) for FTD group, and 13.8 min (range: 12.5 to 16.5 min) for HC group. Notably, the dataset is publicly accessible online, with each participant having provided informed consent for their data to be published. Since the published data do not contain any personally identifiable information, ethical approval was not required for our study. A summary of the dataset is provided in Table 1.

Pre-processing EEG Signals

- *Noise removing*: The EEG signals underwent several preprocessing steps. Initially, a Butterworth band-pass filter ranging from 0.5 to 45 Hz was applied to enhance signal

Table 1 Summary of the OpenNeuro ds004504 dataset used for the proposed framework

	Subjects	Male/female	Age	Average MMSE	Average recording duration
Normal	29	11/18	67.9 ± 5.4	30	13.8 min
AD	36	13/23	66.4 ± 7.9	17.75 ± 4.5	13.5 min
FTD	23	14/9	63.6 ± 8.2	22.17 ± 8.22	12 min

quality. Afterwards, the signals were re-referenced to A1-A2 for consistency. An Automatic Artifact Rejection (ASR) [32] routine was then implemented to eliminate transient or large-amplitude artifacts [33], identified as data periods exceeding the maximum acceptable 0.5-s window standard deviation of 17. Next, Independent Component Analysis (ICA) using the RunICA algorithm transformed the 19 EEG signals into 19 ICA components. Components labeled as "eye artifacts" or "jaw artifacts" by the automatic classification routine "ICLabel" in the EEGLAB platform were automatically discarded [34]. Following this, the signals were resampled to 256 Hz for standardization.

- *Segmentation*: Finally, the signals were segmented for further analysis. In this segmentation technique, the original EEG data is divided into short, informative fragments. These fragments are then normalized to have the same level as the original signal. By doing so, we increase the data sample size while maintaining an equal ratio [35, 36]. In our study, we have specifically segmented the filtered signals into three-second (3 s) time segments, following similar approaches used in previous studies [35–37]. This choice of 3-s segments offers several advantages: it improves computational efficiency, preserves essential information, and enhances performance in classification tasks [37].
- *Arranging EEG channels by brain lobes*: After segmentation of the EEG signal, we have worked on the channel selection process. In the channel selection process, groups of channels were chosen based on their respective brain lobes to facilitate targeted analysis. Five distinct brain lobes were considered: frontal (comprising Fp1, Fp2, F7, F3, Fz, F4, F8), central (including C3, Cz, C4), temporal (encompassing T3, T4, T5, T6), parietal (consisting of P3, P4, Pz), and occipital (comprising O1, O2, Oz) as shown in Fig. 2. Each group of channels corresponded to the electrical activity recorded from specific regions of the brain, enabling focused examination of activity within these regions.

Additionally, to provide a comprehensive perspective, all channels were collectively considered as a full set for comparative analysis, ensuring that any observed patterns or trends could be evaluated across the entirety of the recorded EEG data. This approach facilitated a nuanced exploration of brain activity across various spatial domains, enhancing the depth and breadth of the EEG analysis.

Converting EEG Signals to Spectrogram Images

In this step, we use a plotting method based on short-time Fourier transform (STFT) to generate spectrogram images from the previously decomposed signal segments. Spectrograms are frequently used for analyzing EEG data in the time–frequency domain [35]. The process involves converting the time-varying EEG signal into a two-dimensional (2D) matrix, where time is represented along the horizontal axis, and frequency is depicted along the vertical axis. The horizontal axis corresponds to time, where the EEG signal is discretized into segments or windows. Meanwhile, the

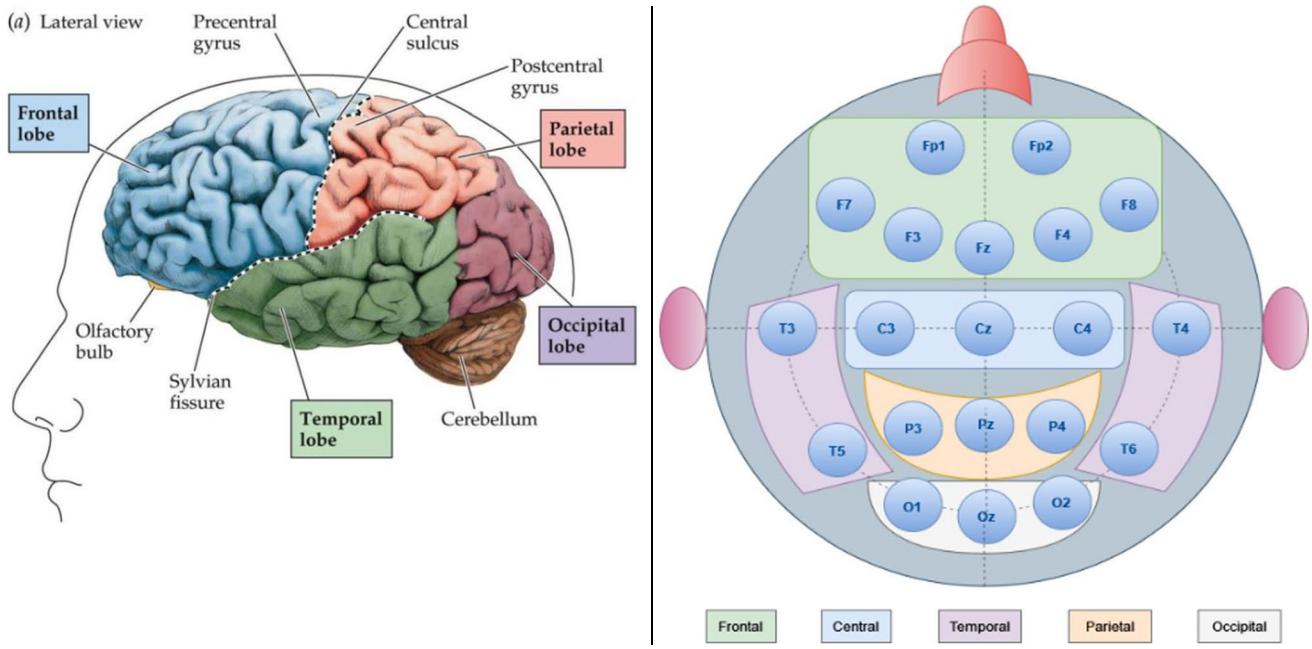

Fig. 2 An illustration of the brain lobe structure showing the arrangement of EEG channels

vertical axis represents the frequency range, typically commencing with lower frequencies at the base and extending upward to higher frequencies.

Within the spectrogram, individual data points correspond to specific time instances and frequencies. The color or intensity of each point serves as an indicator of the power or magnitude of the associated frequency component at that particular moment. Darker or less intense areas represent lower power or the absence of certain frequency components, while brighter or more intense areas reflect higher power and the presence of those frequency components [35]. The STFT works by splitting the signal into overlapping, windowed segments. A Hamming window is applied to each segment to ensure continuity and reduce spectral leakage. Subsequently, the Fourier transform is applied to each windowed segment, yielding its localized frequency spectrum. The STFT of a signal at a given time t and frequency f, represented as STFT(t, f), is computed using the following equation:

$$\mathrm{STFT}(t,f) = \int_{-\infty}^{\infty} x(\tau)\omega(t-\tau)e^{-j2\pi f\tau}d\tau \tag{1}$$

where $x(\tau)$ represents the original signal, $\omega(t—\tau)$ denotes the window function, and f stands for frequency. In summary, the STFT-based spectrogram provides valuable insights into the time–frequency characteristics of EEG signals, aiding in the analysis and classification of brain activity patterns [35].

Classification of Dementia: Training the CNN Model with Spectrogram Images

In this study, we employed a DL-based CNN model to classify the generated spectrogram images. CNNs are highly regarded in the field of deep learning for their remarkable ability to perform image classification tasks efficiently [38]. They excel in this domain by autonomously identifying and extracting relevant features from input images, thereby enabling accurate classification into multiple categories [23, 35, 38].

The strength of CNNs lies in their architectural design, which includes multiple convolutional layers. These layers are instrumental in the feature learning process, as they can detect both low-level features, such as edges, corners, and textures, and high-level features, such as complex shapes and semantic representations. This multi-layered approach allows CNNs to build a hierarchical understanding of the visual data [23, 38]. Specifically, the initial layers of a CNN capture basic visual elements (low-level features) that are foundational to the image, such as edges and textures. As the data progresses through the network, deeper layers combine these basic elements into more complex patterns and features (high-level features), ultimately enabling the model to recognize intricate and abstract visual patterns and objects [38].

This hierarchical feature learning is crucial for the CNN's ability to comprehend and classify complex visual inputs accurately. By leveraging this structured approach, CNN can effectively discern and categorize spectrogram images, which are visual representations of EEG signals, into their respective classes. The capability to understand and process such complex patterns makes CNNs exceptionally powerful tools for a wide range of image classification applications [23, 35].

The convolution operation is essential in CNNs, crucial for extracting meaningful features from images, enabling tasks like image classification and object detection. The operation in a convolutional layer, which utilizes a spatial filter with dimensions $M \times N$ and C channels, can be expressed as follows:

$$Y_{i,j,k} = f\left(\sum_{m=1}^{M}\sum_{n=1}^{N}\sum_{c=1}^{C} X_{i+m-1,j+n-1,c}.W_{m,n,c,k} + b_k\right) \tag{2}$$

In this equation, $Y_{i,j,k}$ represents the value at the i^{th} row, j^{th} column, and k^{th} channel of the output feature map; $X_{i+m-1,j+n-1,c}$ corresponds to the value at the $(i+m-1)^{\text{th}}$ row, $(j+n-1)^{\text{th}}$ column, and c^{th} channel of the input feature map; $W_{\text{m,n,c,k}}$ denotes the filter weight located at m^{th} row, n^{th} column, and c^{th} channel for the k^{th} output channel; b_k represents the bias term associated with the k^{th} output channel; and $f(.)$ refers to the activation function, which is applied to the summation result to introduce non-linearity into the model. This equation computes the dot product between the filter weights and a local region of the input feature map, then adds the bias and applies the activation function, enabling the network to capture complex patterns and features in the image.

In our spectrogram image classification endeavors, we employed the CNN model that we previously proposed and applied in our earlier research [23, 35]. This consistent approach allowed us to build upon our prior findings and maintain continuity in our methodology. This CNN model was initially introduced in [35] for classifying autism spectrum disorder (ASD) using spectrogram images and was later applied to identify frequency band-based biomarkers in EEG signals for the detection of MCI. The architecture of this model consists of four convolutional layers, three dropout layers, a fully connected layer, and a final classification layer, as illustrated in Fig. 3.

Each convolutional layer (Conv) in the model contains 32 filters, each with a kernel size of 3×3, and is followed by a max pooling layer to reduce spatial dimensions. Additionally, the second and fourth pairs of convolutional and max pooling layers are followed by dropout layers with a dropout rate of 25%, which helps to prevent overfitting. The fully connected layer, which serves to integrate the features

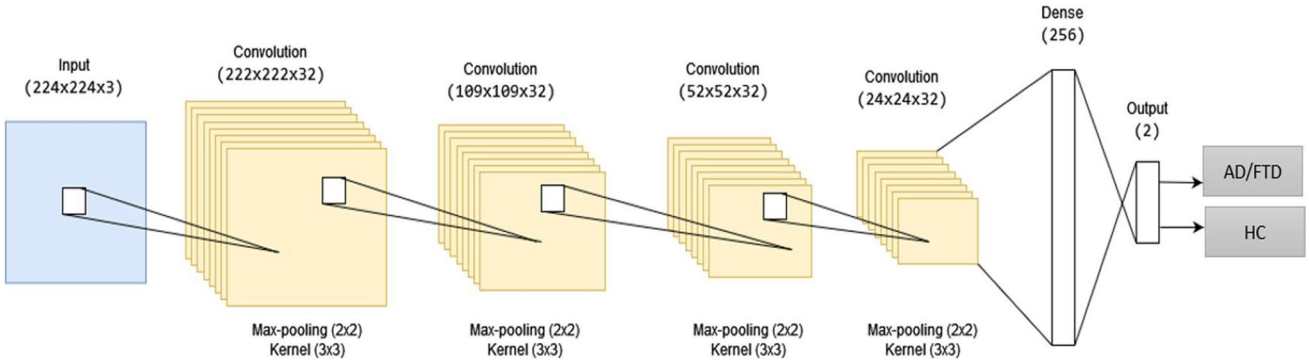

Fig. 3 Proposed architecture of our CNN model

extracted by the convolutional layers, is followed by a dropout layer with a higher dropout rate of 50%. The final classification layer uses a softmax activation function, which outputs probabilities for the two classes: HC or patient. The model is trained using a categorical cross-entropy loss function and optimized with the Adam optimizer, ensuring efficient and effective learning. For a detailed breakdown of the layer configurations, please refer to Table 2.

Performance Evaluation Methods and Metrics

To evaluate our model's performance, we implemented k-fold cross-validation (CV) as our validation technique. In this approach, the dataset is partitioned into k equal-sized segments. The model is trained using $k-1$ of these segments and subsequently tested on the remaining part. This iterative process is repeated k times, with each segment serving as the validation set once. This ensures that every part of the dataset is used for validation exactly one time. After completing these iterations, we average the results to obtain a comprehensive measure of the model's performance. For our study, we specifically employed tenfold cross-validation.

To thoroughly assess the performance of the proposed framework, we quantified six well-known parameters: specificity (Spec), sensitivity (Sen), precision (Prec), accuracy (Acc), $F1$ score ($F1$), and false positive rate (FPR). A receiver operating characteristic (ROC) curve is a graphical representation used to evaluate the diagnostic performance of a binary classifier system. It plots the true positive rate (sensitivity) against the false positive rate (1-specificity) at various threshold settings. The ROC curve is a powerful tool in medical research and machine learning for assessing the ability of a model to distinguish between two classes, such as disease presence versus absence. By visualizing the trade-off between sensitivity and specificity, the ROC curve helps in selecting the optimal threshold for classification and comparing the performance of different models. This makes it an essential tool for evaluating predictive accuracy

Table 2 The configuration of the CNN model used is this study

Layer type	Filters/units	Kernel size	Strides	Activation	Padding	Dropout rate
Input	-	-	-	-	-	-
Conv2D	32	3×3	1×1	ReLU	Same	-
MaxPooling2D	-	2×2	2×2	-	-	-
Conv2D	32	3×3	1×1	ReLU	Same	-
MaxPooling2D	-	2×2	2×2	-	-	-
Dropout	-	-	-	-	-	0.25
Conv2D	32	3×3	1×	ReLU	Same	-
MaxPooling2D	-	2×2	2×2	-	-	-
Conv2D	32	3×3	1×1	ReLU	Same	-
MaxPooling2D	-	2×2	2×2	-	-	-
Dropout	-	-	-	-	-	0.25
Flatten	-	-	-	-	-	-
Dense	256	-	-	ReLU	-	-
Dropout	-	-	-	-	-	0.50
Dense (Output)	2	-	-	Softmax	-	-

in various applications, particularly in diagnostic tests and classification problems [18, 39].

Experiments and Results

This section begins by describing the experimental setup, followed by a thorough presentation of the results. It concludes with an in-depth analysis of the outcomes achieved.

Experimental Setup

Here, we have used dataset with three different categories of subjects and have carried out two different classification tasks: AD vs. HC and FTD vs. HC. We have used a segmentation length of 3-s, consistent with the approach used in prior research [23, 35–37]. Then, we have generated the spectrogram image from those signal segments using STFT. After these segmentation and image generation steps the resulting dataset contains 9695 images of AD subjects, 5546 images of FTD subjects, and 8024 images of HC subjects. The dimension of those images are 224×224 pixels and are then used as input for the CNN model. We have also followed the same process for different brain regions to generate the spectrogram images by using the channel data of those regions. The experiments were conducted on a computer equipped with an AMD Threadripper Pro processor, boasting 256 GB of RAM and 48 GB of graphics memory. During training, we have employed 50 epochs with a training batch size of 32 to train the CNN model.

Results

In this research work, we have devised a framework to find out the critical brain lobes of EEG signal data for dementia disease detection. We have conducted two classification tasks to check the performance of the proposed framework: AD vs. HC and FTD vs. HC. We have used tenfold CV to validate the experimental results. Table 3 reports the tenfold average result of the experiments for different brain lobes for the considered evaluation parameters.

From Table 3, we can see that, using full brain region with the proposed framework, we have achieved an accuracy of 95.59% with a standard deviation of ± 0.46 over tenfold in AD vs. HC classification. On the other hand, for FTD vs. HC, we have achieved an accuracy of 93.14% with a standard deviation of ± 0.93. Among the tested five brain lobes, for AD vs. HC, we have achieved an accuracy of 55.91 ± 2.71, 74.84 ± 10.84, 76.61 ± 1.51, 92.25 ± 0.89, and 78.77 ± 8.26 for Central, Frontal, Occipital, Parietal, and Temporal lobes, respectively. For FTD vs. HC, those values are 64.97 ± 2.93, 82.32 ± 1.13, 77.13 ± 2.18, 95.72 ± 0.42, and 79.34 ± 1.89, accordingly.

Table 3 Average performance (%) and standard deviation of the proposed framework in tenfold cross-validation across different brain lobes for AD vs. HC and FTD vs. HC classification tasks

Brain lobes		AD vs. HC	FTD vs. HC
Full brain region	**Sensitivity**	97.37 ± 0.80	92.03 ± 1.38
	Specificity	93.42 ± 1.24	93.92 ± 1.34
	Precision	94.73 ± 0.84	91.29 ± 1.79
	***F*1**	96.00 ± 0.00	92.00 ± 0.01
	Accuracy	$\mathbf{95.59 \pm 0.46}$	$\mathbf{93.14 \pm 0.93}$
	FPR	6.00 ± 1.24	5.77 ± 1.34
Central (C3, Cz, C4)	**Sensitivity**	97.57 ± 7.28	37.62 ± 19.32
	Specificity	5.09 ± 15.26	83.65 ± 8.67
	Precision	55.77 ± 2.32	49.19 ± 24.64
	***F*1**	71.00 ± 0.01	42.00 ± 0.21
	Accuracy	55.91 ± 2.71	64.97 ± 2.93
	FPR	100.00 ± 15.26	17.21 ± 8.67
Frontal (Fp1, Fp2, F7, F3, Fz, F4, F8)	**Sensitivity**	83.13 ± 9.18	72.21 ± 2.88
	Specificity	65.35 ± 32.70	89.31 ± 0.98
	Precision	77.93 ± 12.27	82.26 ± 1.83
	***F*1**	79.00 ± 0.05	77.00 ± 0.02
	Accuracy	74.84 ± 10.84	82.32 ± 1.13
	FPR	34.81 ± 32.70	10.32 ± 0.98
Occipital (O1, O2, Oz)	**Sensitivity**	83.52 ± 1.49	74.13 ± 4.56
	Specificity	68.24 ± 3.22	79.17 ± 3.15
	Precision	76.11 ± 1.83	71.13 ± 2.41
	***F*1**	80.00 ± 0.01	73.00 ± 0.03
	Accuracy	76.61 ± 1.51	77.13 ± 2.18
	FPR	32.92 ± 3.22	19.60 ± 3.15
Parietal (P3, P4, Pz)	**Sensitivity**	89.67 ± 1.44	92.79 ± 1.27
	Specificity	95.38 ± 0.77	97.75 ± 0.49
	Precision	95.90 ± 0.70	96.59 ± 0.71
	F1	93.00 ± 0.01	95.00 ± 0.00
	Accuracy	$\mathbf{92.25 \pm 0.89}$	$\mathbf{95.72 \pm 0.42}$
	FPR	4.17 ± 0.77	2.25 ± 0.49
Temporal (T3, T4, T5, T6)	**Sensitivity**	86.94 ± 5.09	73.59 ± 3.51
	Specificity	68.91 ± 23.15	83.34 ± 2.26
	Precision	78.85 ± 8.34	75.29 ± 2.65
	***F*1**	82.00 ± 0.04	74.00 ± 0.02
	Accuracy	78.77 ± 8.26	79.34 ± 1.89
	FPR	23.48 ± 23.15	17.23 ± 2.26

To further analyze the comparison of the considered parameters in different lobes, we have plotted lobe-wise sensitivity, specificity, precision, and accuracy in Figs. 4, 5, 6, and 7, respectively. In these figures, we used error bars to visually represent the variability of the performance parameters within two groups: AD vs. HC and FTD vs. HC. The error bars illustrate the range of variation within each group, providing insight into the consistency of performance across

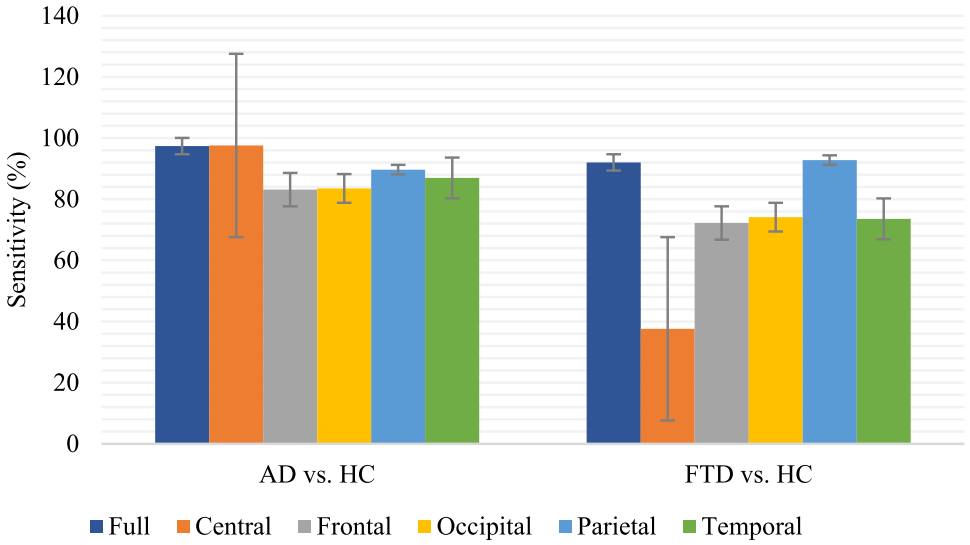

Fig. 4 Sensitivity comparison across different brain regions for AD vs. HC and FTD vs. HC classification

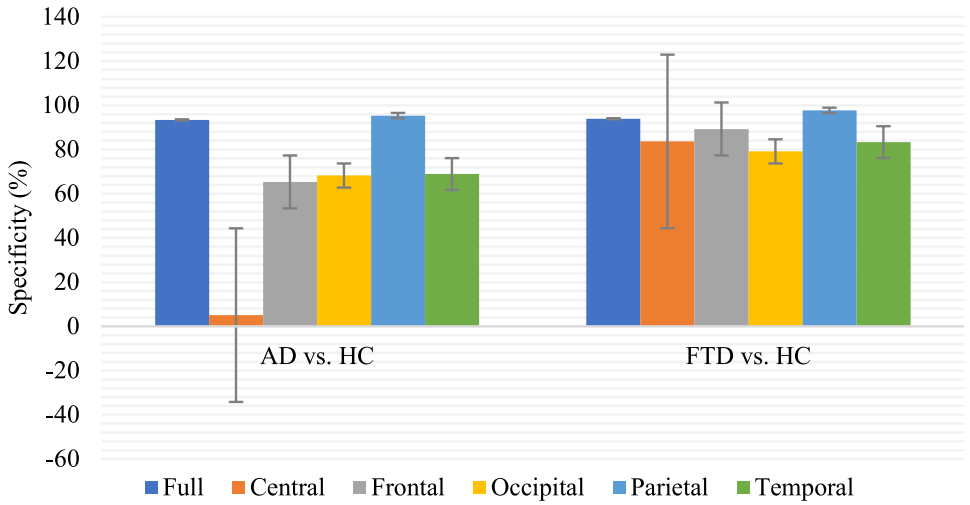

Fig. 5 Specificity comparison across different brain regions for AD vs. HC and FTD vs. HC classification

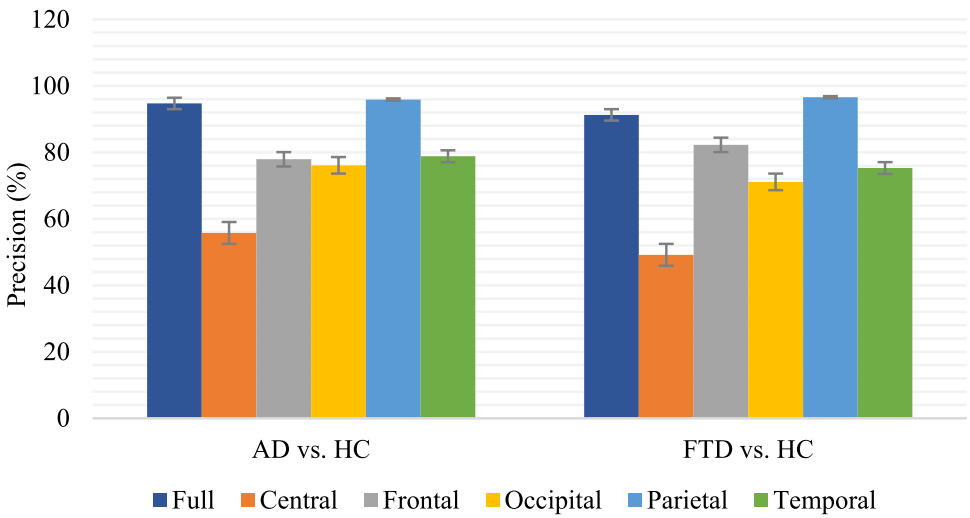

Fig. 6 Precision comparison across different brain regions for AD vs. HC and FTD vs. HC classification

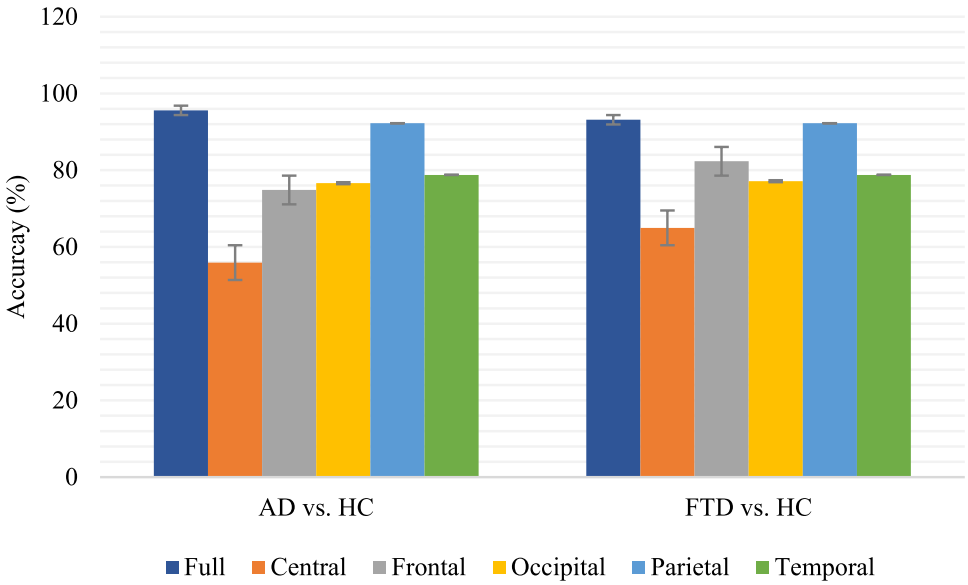

Fig. 7 Accuracy comparison across different brain regions for AD vs. HC and FTD vs. HC classification

the two groups. This helps in understanding how reliable and stable the observed performance metrics are within each comparison.

Figure 4 shows the lobe-wise comparison for the sensitivity values in both AD vs. HC and FTD vs. HC classification. From Fig. 4, we can see that, for AD vs. HC with full brain region, we have achieved an average sensitivity of 97.37% and for FTD vs. HC, it is 92.03%. On the other hand, among the five brain lobes, central lobe has given the highest sensitivity value of 97.57% for AD vs. HC classification, which is higher than the full brain region. Other regions like parietal and temporal also show high sensitivity, while the frontal and occipital regions display comparatively lower sensitivity. In case of FTD vs. HC, parietal lobe has generated the highest average sensitivity of 92.79%, which is also better than the full brain region. The error bars in Fig. 4 indicate that there are no significant differences in sensitivity across the various lobes between the two groups, with the exception of the central lobe. Notably, the central region shows a markedly low sensitivity of 37.62%, suggesting it is less effective in identifying FTD. Overall, this comparison highlights the varying diagnostic value of different brain regions, emphasizing the importance of region-specific analysis in accurately distinguishing between these neurodegenerative diseases and healthy states.

Figure 5 illustrates the specificity percentages for different brain regions in distinguishing AD from HC and FTD from HC. For AD vs. HC, the parietal region demonstrates the highest specificity at 95.38%, followed closely by the full region at 93.42%. The central region shows a notably low specificity of 5.09%, indicating poor effectiveness in ruling out AD when it is not present, which results in a low overall classification accuracy for this region despite producing the highest sensitivity value. Other regions like the frontal, occipital, and temporal regions exhibit moderate specificity levels. In the context of FTD vs. HC, the parietal and full regions again show high specificity at 97.75% and 89.31%, respectively, suggesting their robustness in distinguishing FTD from healthy controls. Similar to Fig. 4, Fig. 5 also shows that the variation in specificity across the various lobes between the two groups is consistent, with the exception of the central lobe. The central region displays improved specificity for FTD vs. HC at 83.65% compared to its performance in AD vs. HC. The frontal and temporal regions show relatively high specificity, while the occipital region exhibits moderate specificity. This comparison highlights the variability in specificity across different brain regions and underscores the significance of selecting appropriate regions for accurate differentiation between neurodegenerative diseases and healthy states.

Figure 6 illustrates the precision percentages for different brain regions in AD vs. HC and FTD vs. HC. In the AD vs. HC comparison, the full brain and parietal region analysis yields a high precision of 94.73% and 95.9%, respectively, while the central region shows a significantly lower precision of 55.77%. The occipital, frontal, and temporal regions show moderate precision values of 76.11%, 77.93%, and 78.85%, respectively. In the FTD vs. HC comparison, the parietal analysis again shows a high precision of 96.59% followed by full brain with 91.29%, with the central region lagging at 49.19%. The frontal, occipital, and temporal regions display precisions of 82.26%, 71.13%, and 75.29%, respectively. Overall, the full brain analysis and parietal region consistently exhibit high precision, while the central region consistently underperforms in both comparisons. Figure 6 reveals that the variation in precision across the different lobes between the two groups is stable.

Figure 7 provides a comparative analysis of the accuracy percentages for different brain regions in distinguishing AD vs. HC and FTD vs. HC. For AD vs. HC comparison, the full brain region demonstrates the highest accuracy, with 95.59%. Conversely, the central region shows the lowest accuracy, with 55.91%. Among other regions, the parietal region shows high accuracy of 92.25%, while the frontal, temporal, and occipital regions display moderate accuracy levels. On the other hand, for FTD vs. HC, parietal region achieved higher accuracy (95.72%) than the full region (93.14%). Like the AD vs. HC, the central region again shows the lowest accuracy, with 64.97% and other three regions have produced moderate accuracy level. This comparison highlights the variability in diagnostic accuracy across different brain regions, emphasizing the superior performance of the full and parietal regions in both conditions. Figure 7 also shows that the variation in accuracy across the different lobes between the two groups is consistent.

Figure 8 is the ROC curve illustrating the performance of classifier across different brain regions for AD vs. HC. Each line on the graph represents a different brain region, and the curve plots the true positive rate (sensitivity) against the false positive rate (1-specificity). The full brain analysis (green line) shows an almost perfect performance with a sharp rise and high positioning close to the top-left corner, indicating high sensitivity and low false positive rate. The parietal region (blue line) also shows excellent performance, closely following the full brain analysis. Other regions like frontal (yellow), occipital (green), and temporal (brown) show moderate performance with some variability but still demonstrate relatively high true positive rates with acceptable false-positive rates. The central region (dark blue line) deviates significantly, indicating poorer performance with a higher false positive rate. Overall, the graph emphasizes the superior performance of the full brain and parietal regions in distinguishing AD from HC.

The ROC curve presented in Fig. 9 illustrates the performance of the classifier across various brain regions for distinguishing FTD from HC. The full brain analysis (green line) shows an almost ideal performance with a steep rise and positioning close to the top-left corner, indicating high sensitivity and low false positive rate. The parietal region (blue line) also demonstrates excellent performance, closely following the full brain curve with high sensitivity and low false-positive rates. Other regions, such as the frontal (yellow), occipital (green), and temporal (brown), exhibit moderate performance, showing variability but maintaining relatively high true positive rates with acceptable false positive rates. The central region (dark blue line), however, deviates significantly, indicating poor performance with a higher false positive rate and lower sensitivity. Overall, the graph highlights the superior performance of the full brain and parietal regions in differentiating FTD from HC, while the central region shows substantial limitations in classification accuracy.

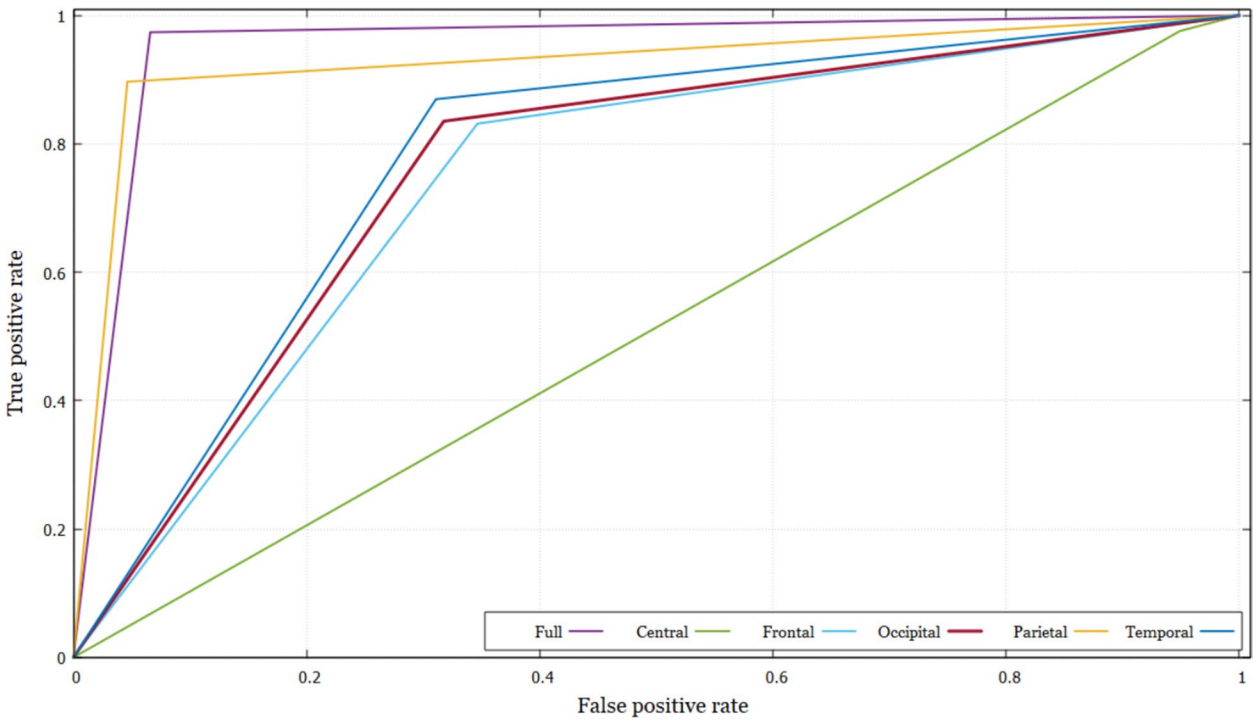

Fig. 8 ROC curve for AD vs. HC classification for different brain regions

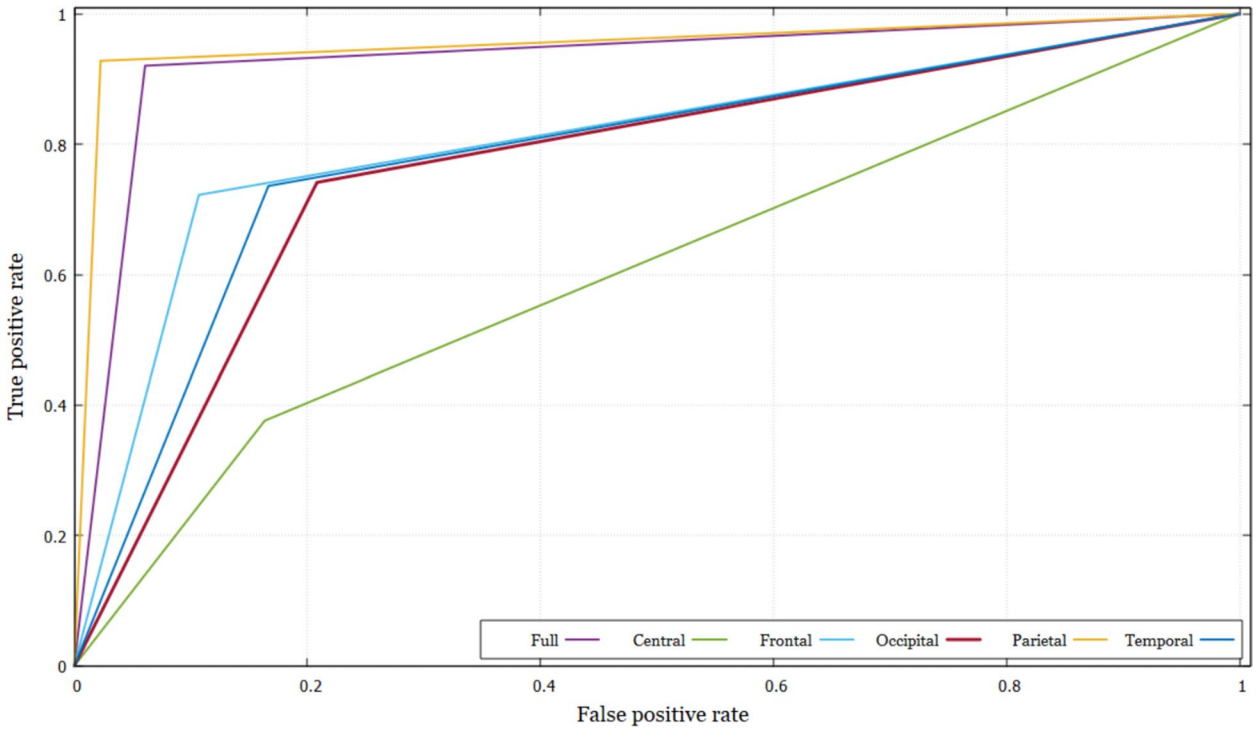

Fig. 9 ROC curve for FTD vs. HC classification for different brain regions

Figure 10 presents confusion matrices for binary classification tasks involving AD vs. HC and FTD vs. HC. Each matrix shows the distribution of predictions: true positives (P), true negatives (N), false positives, and false negatives. The varying classification performances indicate the diagnostic significance of these regions, with differences in sensitivity and specificity contributing to insights into the role of each region in distinguishing between the conditions.

Discussion

This study presents a novel framework combining STFT and CNN to identify key brain lobes as biomarkers for detecting AD and FTD using EEG data. In the framework, firstly EEG signals were pre-processed using a Butterworth band-pass filter, automatic artifact rejection, and Independent Component Analysis (ICA) to remove various artifacts and noise.

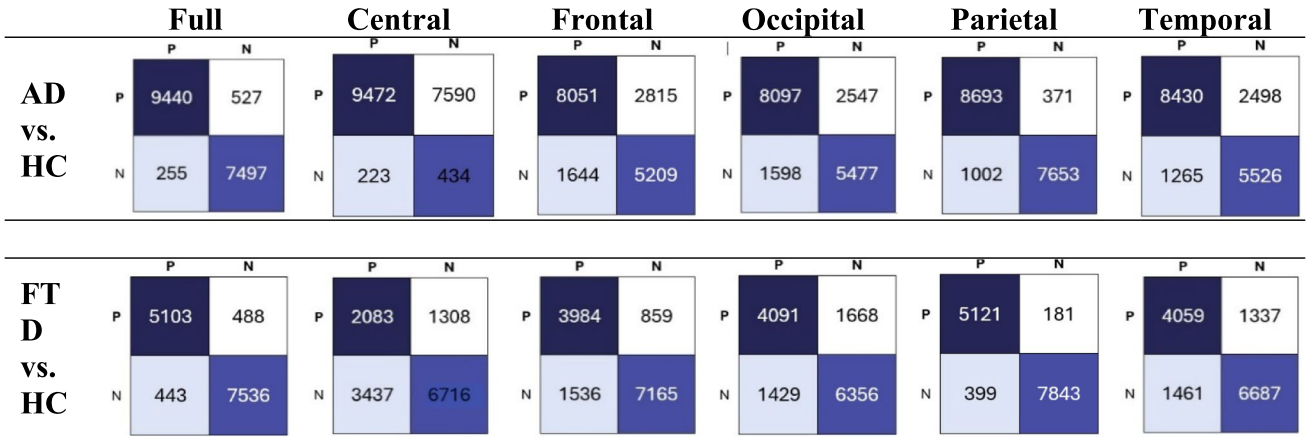

Fig. 10 Confusion matrices for binary classification tasks comparing AD and HC (1st row) and FTD and HC (2nd row) across different brain regions: full, central, frontal, occipital, parietal, and temporal. Each confusion matrix displays the true positives (P) and true negatives (N) for the respective comparisons

The signals were then segmented into three-second (3 s) time frames, following established research [35–37]. Next, EEG channels were grouped based on their corresponding brain lobes-frontal (Fp1, Fp2, F7, F3, Fz, F4, F8), central (C3, Cz, C4), temporal (T3, T4, T5, T6), parietal (P3, P4, Pz), and occipital (O1, O2, Oz) to facilitate targeted analysis. The EEG signals were then converted into spectrogram images using STFT, providing a time–frequency representation of brain activity for each brain lobe and the full EEG channel set. These spectrograms were subsequently fed into a deep learning-based CNN trained to classify dementia. Two classification tasks—AD vs. HC and FTD vs. HC—were conducted to evaluate the proposed approach. Classification was performed separately for each brain lobe's spectrograms and the full channel set to assess their effectiveness in dementia detection. The framework was evaluated using the OpenNeuro ds004504 EEG dataset, demonstrating its effectiveness in accurate and lobe-specific dementia classification. As per results in Table 3 and Fig. 7, the proposed method achieved a 95.59% classification accuracy for AD vs. HC using the full brain region and 95.72% for FTD vs. HC in the parietal lobe. The ROC graph in Fig. 8 demonstrates that our proposed STFT-based CNN model achieves superior performance in distinguishing AD from HC, particularly in the full brain and parietal regions. Similarly, Fig. 9 highlights the model's strong performance in differentiating FTD from HC, with the full brain and parietal regions showing the highest accuracy.

The EEG signals from various brain regions provide critical insights into the neural dysfunctions associated with AD. Each brain region contributes uniquely to the diagnostic process, and understanding these contributions helps improve the accuracy and reliability of EEG-based AD detection [37–43]:

- The temporal lobe, particularly the hippocampus, plays a significant role in memory and cognitive functions, which are severely affected in AD. EEG studies have shown that AD patients exhibit reduced alpha and beta power in the temporal regions, along with increased theta and delta activity, indicating neural deterioration. These changes are crucial for early detection as they correlate strongly with the hallmark symptoms of AD. In this study, we have also found that using temporal region EEG data, we achieved an accuracy of 78.77% for AD vs. HC and 79.34% for FTD vs. HC classification. These are the second and third highest classification accuracy for the two classifications, accordingly.
- The parietal lobe is involved in integrating sensory information and spatial navigation. EEG signals from the parietal region in AD patients often show decreased alpha activity and increased theta activity. This disruption in normal brain rhythms is associated with impaired cognitive and spatial processing abilities, making parietal EEG signals important for detecting AD-related changes. Here, we have achieved the highest accuracy among the tested five brain regions for both the classification tasks. Even we have achieved better accuracy (95.72%) using parietal brain region than using the full brain region (93.14%) for FTD vs. HC classification.
- The frontal lobe is associated with executive functions, such as decision-making and problem-solving. EEG recordings from the frontal region in AD patients typically show decreased beta power and increased theta and delta power. These alterations reflect the decline in cognitive control and executive functions, which are critical for comprehensive AD diagnostics. This is also supported by our study as we have obtained a moderate accuracy using frontal lobe.
- The occipital lobe, responsible for visual processing, shows less pronounced changes in the early stages of AD. However, EEG studies indicate that AD patients may exhibit reduced alpha activity and increased slow-wave activity in the occipital regions as the disease progresses. Including occipital EEG signals can enhance the detection of AD, especially in its later stages. Our obtained results again support this claim by gaining a significant classification accuracy for the classification tasks.
- EEG signals from the central brain regions, including the sensorimotor cortex, are less commonly associated with primary AD symptoms. However, these regions can still show changes in brain rhythms, such as altered mu rhythms, which may reflect broader neural network disruptions in AD. While central EEG signals may not be as diagnostic as those from other regions, they can still contribute to a holistic understanding of AD progression. This is also exhibited in our research work as we have got the lowest classification accuracy using this brain region. We have achieved 55.91% and 64.97% accuracy for AD vs. HC and FTD vs. HC classification, respectively.

Therefore, based on the results, the identified important brain lobes align with prior research findings [40–45].

To identify the most influential spectrogram features in the model's decisions, we applied Grad-CAM method. Figure 11 presents sample spectrogram images from different brain lobes along with their corresponding Grad-CAM visualizations for both classification tasks (AD vs. HC and FTD vs. HC). From the figure, we can see that for the full brain region and parietal lobe, the GRAD-CAM images have significant regions with high heatmap area. Frontal, occipital, and temporal brain lobes also have significant areas with differences in the GRAD-CAM images, but for the central lobe, the GRAD-CAM images also have very few areas with distinguishable markers, which is why its classification performance is low for the classification task.

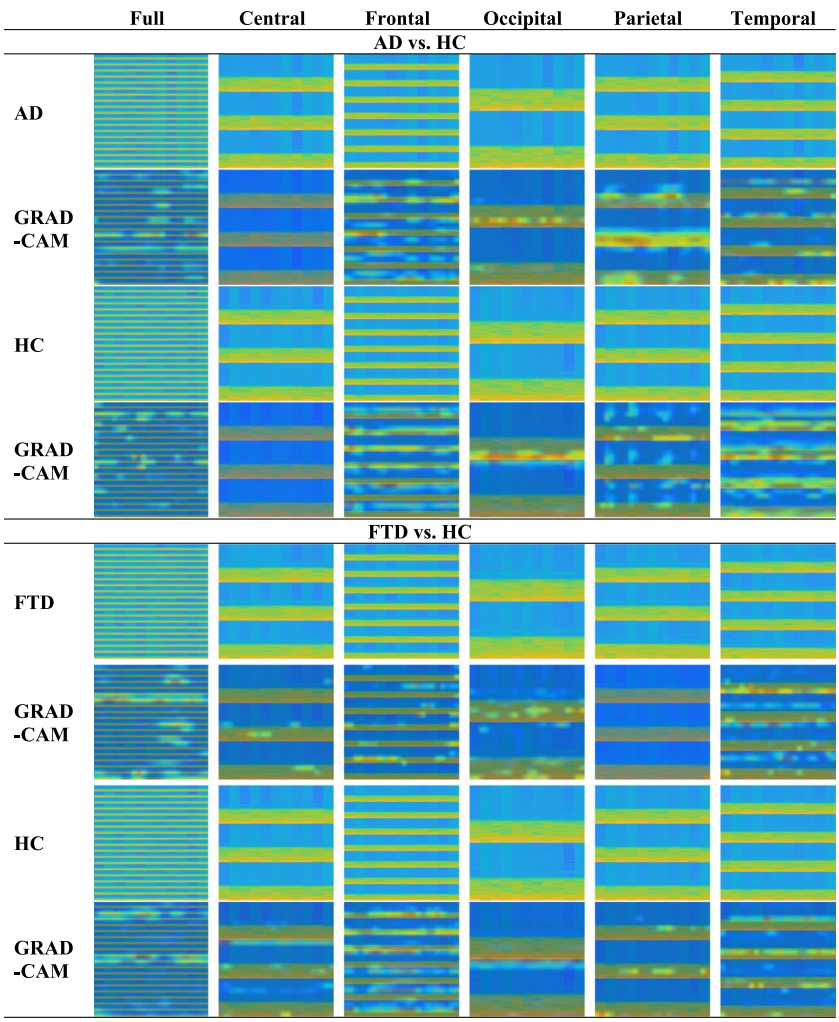

Fig. 11 Sample spectrogram image and their corresponding GRAD-CAM images. First four rows are for AD vs. HC classification and the bottom four rows are for FTD vs. HC classification. Here, odd rows are spectrogram images for different brain lobes and the even rows are their corresponding GRAD-CAM images

To ensure a comprehensive comparison between our framework and existing state-of-the-art (SoA) studies using the OpenNeuro ds004504 dataset, we have compiled and presented a detailed comparative analysis in Table 4. By presenting this side-by-side comparison, we aim to highlight the effectiveness and advancements of our approach in relation to established methodologies.

Miltiadous et al. [31] introduced a Dual-Input Convolution Encoder Network (DICE-net) for classifying EEG data related to AD. DICE-net integrates convolutional layers, a transformer encoder, and feed-forward layers to classify band power and coherence features extracted from denoised signal data. The results showed an accuracy of 83.28% for AD vs. HC classification using Leave-One-Out Validation (LOOV) and 74.96% for FTD vs. HC classification. Chen et al. [45] presented a two-branch network architecture combining CNNs and visual transformers (ViTs) for classifying EEG data to detect AD and FTD. They achieved an accuracy of 87.33% for AD vs. HC classification and 82.98% for FTD vs. HC classification. Miltiadous et al. [6] calculated EEG rhythm energy by applying five bandpass filters (delta, theta, alpha, beta, and gamma) to extract frequency-domain characteristics. Mean, variance, and interquartile range (IQR) were time-domain measures. Six supervised machine learning models for dementia diagnosis were used to assess these features. The best accuracy among them was 78.5% for AD vs. HC for decision trees (C4.5), and 86.3% for FTD detection for random forests. Miltiadous et al. [8] described the OpenNeuro ds004504 dataset, used in this study, containing raw and pre-processed EEG data in BIDS format. The study extracted Relative Band Power (RBP) features and applied SVM, KNN, MLP, and RF for classification, with RF achieving 77.01% accuracy for AD vs. HC and MLP 73.12% for FTD vs. HC.

In [11], Lal et al. evaluated various feature extraction techniques to identify AD and FTD biomarkers from EEG signals. They developed an optimized machine learning framework integrating sliding windowing, feature extraction, and supervised learning to differentiate AD, FTD, and HC. Using singular value decomposition (SVD) entropy for feature extraction and *K*-nearest neighbors (KNN) for classification, their model achieved 91% accuracy for AD vs. HC

Table 4 Comparison with existing studies on AD vs. HC and FTD vs. HC classification for the EEG dataset: OpenNeuro ds004504 dataset (used in this study)

Classification	Study	Method	Segmentation	Validation	Accuracy
AD vs. HC	Miltiadous et al. [31]	DICE-net	30 s with 15 s overlap	LOOV	83.28%
	Chen et al. [45]	Combining CNNs and visual transformers	4 s	tenfold	87.33%
	Miltiadous et al. [6]	Energy, mean, variance, IQR, decision trees	5 s	LOOV	78.50%
	Lal et al. [11]	SVD entropy based KNN	1 s	15-fold	91.00%
	Parihar and Swami [46]	Frequency band analysis with EL	–	15-fold	93.60%
	Mootoo et al. [7]	Graph-based SVM	–	twofold	85%
	Miltiadous et al.[8]	RBP-based random forests	4 s	LOOV	77.01%
	Proposed work	Short-time Fourier transform-based CNN	3 s	tenfold	**95.59%**
FTD vs. HC	Miltiadous et al. [31]	DICE-net	30 s with 15 s overlap	LOOV	74.96%
	Chen et al. [45]	Combining CNNs and visual transformers	4 s	tenfold	82.98%
	Miltiadous et al.[6]	Energy, mean, variance, IQR, random forests	5 s	LOOV	86.30%
	Lal et al. [11]	SVD entropy based KNN	1 s	15-fold	93.00%
	Parihar and Swami [46]	Variance and Kurtosis with EL	–	15-fold	87.00%
	Miltiadous et al. [8]	RBP-based MLP	4 s	LOOV	73.12%
	Proposed work	Short-time Fourier transform-based CNN	5 s	tenfold	**95.72%**

Note: "–" indicates "not reported in the paper"

and 93% for FTD vs. HC. Parihar and Swami [46] utilized EEG features from multiple frequency bands (delta, theta, alpha, beta, and gamma) with an Ensemble Bagged Learning (EL) algorithm to classify subjects as healthy, AD, or FTD. Their approach achieved 93.6% accuracy for AD vs. HC and 87.0% for FTD vs. HC. Mootoo et al. [7] applied Graph Signal Processing (GSP) techniques using the Graph Discrete Fourier Transform (GDFT) to analyze EEG recordings for AD detection, leveraging various machine learning and deep learning models. The results demonstrated that the SVM classifier achieved the highest accuracy of 85% for AD vs. HC.

As shown in Table 4, our study achieved superior accuracy compared to all previous studies that utilized the OpenNeuro ds004504 dataset. This demonstrates the strong capability of our STFT-based CNN framework in identifying different forms of dementia, including AD and FTD, using EEG signals. These results highlight the effectiveness of our approach and its potential to establish a new benchmark in the field.

Conclusions and Future Plan

In this research, we developed a framework for identifying critical brain lobes for dementia detection, specifically focusing on the classification of AD and FTD from HC subjects using EEG data. Initially, the EEG signals were segmented into three-second time frames, and these segments were then transformed into spectrogram images using STFT. A CNN model is used to train and classify those spectrogram images into corresponding classes. We have tested our model on two classification tasks: AD vs. HC and FTD vs. HC. We have used this process for full brain region as well as five different brain regions to identify the important brain region in dementia detection. By examining EEG data from a publicly available dataset with AD, FTD, and HC, we have identified that the parietal lobe exhibits the most significant changes in both AD and FTD, followed by the temporal and frontal lobes. In addition, we have used GradCAM method to enhance the interpretability of our results and provide meaningful insights for the research community. These findings emphasize the importance of targeting specific brain lobes in the development of diagnostic and monitoring tools for these neurodegenerative disorders.

The ability to detect abnormalities in the parietal, temporal, and frontal lobes through non-invasive EEG techniques offers a promising avenue for improving early diagnosis and intervention strategies. This approach not only enhances our understanding of the pathological progression of AD and FTD but also has the potential to significantly impact patient outcomes by facilitating timely and accurate diagnosis.

Our research contributes to the growing body of evidence supporting the use of EEG as a valuable tool in the clinical management of neurodegenerative diseases. By pinpointing the brain regions most affected by AD and FTD, we pave the way for more targeted and effective therapeutic interventions. Future studies should continue to explore the utility of EEG in detecting and monitoring these disorders, ultimately aiming to integrate this technology into routine clinical practice for the benefit of patients worldwide.

Author Contribution Siuly Siuly: Conceptualization, Methodology, Writing original draft.

Md. Nurul Ahad Tawhid: Experimental works, validation and writing the description of the results.

Yan Li: Project Supervision.

Rajendra Acharya: review and editing.

Muhammad Tariq Sadiq: review and editing.

Hua Wang: Project Supervision.

Funding Open Access funding enabled and organized by CAUL and its Member Institutions. This work was supported by the 2022 UniSQ Research Capacity Building Grant (Project No. 1008316).

Data Availability No datasets were generated or analysed during the current study.

Declarations

Competing Interests The authors declare no competing interests.

References

1. Australian Institute of Health and Welfare. Dementia in Australia. 2024. https://www.aihw.gov.au/reports/dementia/dementia-in-aus/contents/summary. Accessed 13 Sep 2024.
2. World Health Organization. Dementia. 2023. https://www.who.int/news-room/fact-sheets/detail/dementia. Accessed 15 Mar 2023.
3. Alzheimer's Disease International. Dementia statistics. 2023. https://www.alzint.org/about/dementia-facts-figures/dementia-statistics/.
4. Siuly S, Alçin OF, Wang H, Li Y, Wen P, Zhang Y. Exploring rhythms and channels-based EEG biomarkers for early detection of Alzheimer's disease. IEEE Trans Emerg Top Comput Intell. 2024;8(2):1609–23.
5. Sharma R. Localization of epileptic surgical area using automated hybrid approach based on higher-order statistics with sensitivity analysis and residual wavelet transform. Biomed Signal Process Control 2023;86:105192.
6. Miltiadous A, Tzimourta KD, Giannakeas N, Tsipouras MG, Afrantou T, Ioannidis P, Tzallas AT. Alzheimer's disease and frontotemporal dementia: a robust classification method of EEG signals and a comparison of validation methods. Diagnostics. 2021;11(1437). https://doi.org/10.3390/diagnostics11081437
7. Mootoo et al. Detecting Alzheimer disease in EEG data with machine learning and the graph discrete Fourier transform. 2023. https://doi.org/10.1101/2023.11.01.23297940.
8. Miltiadous A, Tzimourta KD, Afrantou T, Ioannidis P, Grigoriadis N, Tsalikakis DG, Angelidis P, Tsipouras MG, Glavas E, Giannakeas N, et al. A dataset of scalp EEG recordings of Alzheimer's disease, frontotemporal dementia and healthy subjects from routine EEG. Data. 2023;8:95. https://doi.org/10.3390/data8060095.
9. Puri D, Nalbalwar S, Nandgaonkar A, Kachare P, Rajput J, Wagh A. Alzheimer's disease detection using empirical mode decomposition and Hjorth parameters of EEG signal. In 2022 International Conference on Decision Aid Sciences and Applications (DASA). IEEE. 2022;23–28. https://doi.org/10.1109/DASA54658.2022.9765111.
10. Dogan S, Baygin M, Tasci B, Loh HW, Barua PD, Tuncer T, ... Acharya UR. Primate brain pattern-based automated Alzheimer's disease detection model using EEG signals. Cogn Neurodyn. 2022;17(3):647–659.
11. Lal U, Chikkankod AV, Longo L. A comparative study on feature extraction techniques for the discrimination of frontotemporal dementia and Alzheimer's disease with electroencephalography in resting-state adults. Brain Sci. 2024;14:335. https://doi.org/10.3390/brainsci14040335.
12. Briels CT, Schoonhoven DN, Stam CJ, de Waal H, Scheltens P, Gouw AA. Reproducibility of EEG functional connectivity in Alzheimer's disease. Alzheimers Res Ther. 2020;12:1–14.
13. Sheng J, Shao M, Zhang Q, Zhou R, Wang L, Xin Y. Alzheimer's disease, mild cognitive impairment, and normal aging distinguished by multi-modal parcellation and machine learning. Sci Rep. 2020;10(1):1–10.
14. Mammone N, De Salvo S, Bonanno L, Ieracitano C, Marino S, Marra A, Bramanti A, Morabito FC. Brain network analysis of compressive sensed high-density EEG signals in AD and MCI subjects. IEEE Trans Industr Inf. 2018;15(1):527–36.
15. Şeker M, Özbek Y, Yener G, Özerdem MS. Complexity of EEG dynamics for early diagnosis of Alzheimer's disease using permutation entropy neuromarker. Comput Methods Programs Biomed. 2021;206:106116.
16. Tzimourta KD et al. EEG window length evaluation for the detection of Alzheimer's disease over different brain regions. Brain Sci. 2019;9(4). https://doi.org/10.3390/brainsci9040081
17. Fraga FJ, Mamani GQ, Johns G, Tavares TH, Falk TH, Phillips NA. Early diagnosis of mild cognitive impairment and Alzheimer's with event-related potentials and event-related desynchronization in N-back working memory tasks. Comput Methods Programs Biomed. 2018;164:1–13.
18. Siuly S, Alçin OF, Kabir E, Şengür A, Wang H, Zhang Y, Whittaker F. A new framework for automatic detection of patients with mild cognitive impairment using resting-state EEG signals. IEEE Trans Neural Syst Rehabil Eng. 2020;28(9):1966–76.
19. Khare SK, Rajendra Acharya U. Adazd-Net: automated adaptive and explainable Alzheimer's disease detection system using EEG signals. Knowl-Based Syst. 2023;278:110858.
20. Alvi AM, Siuly S, Wang H. A long short-term memory based framework for early detection of mild cognitive impairment from EEG signals. IEEE Trans Emerg Top Comput Intell. 2023;7(2):375–88.
21. Ravikanti DK, Saravanan S. EEGAlzheimer'sNet: development of transformer-based attention long short-term memory network for detecting Alzheimer disease using EEG signal. Biomed Signal Process Control. 2023;86(Part C). https://doi.org/10.1016/j.bspc.2023.105318
22. Chaabene S, Haroun Hassan B, Boudaya A, Chaari L, Bouaziz B. New MCI detection method based on transformer and EEG Data. 31st European Signal Processing Conference (EUSIPCO). Helsinki, Finland. 2023;2023:1200–4. https://doi.org/10.23919/EUSIPCO58844.2023.10290024
23. Tawhid MNA, Siuly S, Kabir E, Li Y. Exploring frequency band-based biomarkers of EEG signals for mild cognitive impairment detection. IEEE Trans Neural Syst Rehabil Eng. 2024;32:189–99.
24. Hasoon J, Hamilton CA, Schumacher J, Colloby S, Donaghy PC, Thomas AJ, Taylor JP. EEG functional connectivity differences

predict future conversion to dementia in mild cognitive impairment with Lewy body or Alzheimer disease. Int J Geriatr Psychiatry. 2024;39(9):e6138. https://doi.org/10.1002/gps.6138.
25. Şeker M, Özerdem MS (2024) Dementia rhythms: unveiling the EEG dynamics for MCI detection through spectral and synchrony neuromarkers. Journal of Neuroscience Methods 2024;409:110216. https://doi.org/10.1016/j.jneumeth.2024.110216.
26. Adebisi AT, Lee HW, Veluvolu KC. EEG-based brain functional network analysis for differential identification of dementia-related disorders and their onset. IEEE Trans Neural Syst Rehabil Eng. 2024;32:1198–209. https://doi.org/10.1109/TNSRE.2024.3374651.
27. Sen SY, Cura OK, Yilmaz GC, Akan A. Classification of Alzheimer's dementia EEG signals using deep learning. Transactions of the Institute of Measurement and Control. 2024;0(0). https://doi.org/10.1177/01423312241267046
28. Şeker M, Özerdem MS. Investigating convolutional and transformer-based models for classifying mild cognitive impairment using 2D spectral images of resting-state EEG. Biomedical Signal Processing and Control 2025;105:https://doi.org/10.1016/j.bspc.2025.10766
29. Acharya M, Deo RC, Barua PD, Devi A, Tao X. EEGConvNeXt: A novel convolutional neural network model for automated detection of Alzheimer's disease and frontotemporal dementia using EEG signals. Comput Methods Programs Biomed 2025;262:2025. https://doi.org/10.1016/j.cmpb.2025.108652
30. Miltiadous A, Tzimourta KD, Afrantou T, Ioannidis P, Grigoriadis N, Tsalikakis DG, Angelidis P, Tsipouras MG, Glavas E, Giannakeas N, Tzallas AT. A dataset of 88 EEG recordings from: Alzheimer's disease, Frontotemporal dementia and Healthy subjects. OpenNeuro. 2023. https://doi.org/10.18112/openneuro.ds004504.v1.0.2.
31. Miltiadous A, Gionanidis E, Tzimourta KD, Giannakeas N, Tzallas AT. Dice-Net: A novel convolution-transformer architecture for Alzheimer detection in EEG signals. IEEE Access. 2023;(99):1–1. https://doi.org/10.1109/ACCESS.2023.3294618.
32. Anders P, Müller H, Skjæret-Maroni N, Vereijken B, Baumeister J. The influence of motor tasks and cut-off parameter selection on artifact subspace reconstruction in EEG recordings. Med Biol Eng Compu. 2020;58:2673–83.
33. Plechawska-Wójcik M, Augustynowicz P, Kaczorowska M, Zabielska-Mendyk E, Zapała D. The influence assessment of artifact subspace reconstruction on the EEG signal characteristics. Appl Sci. 2023;13(3):1605.
34. Delorme A, Makeig S. EEGLAB: an open source toolbox for analysis of single-trial EEG dynamics including independent component analysis. J Neurosci Methods. 2004;134(1):9–21.
35. Tawhid MNA, Siuly S, Wang K, Wang H, Zhang Y. A spectrogram image based intelligent technique for automatic detection of autism spectrum disorder from EEG. PLoS One. 2021;16(6):e0253094.
36. Tawhid MNA, Siuly S, Li T. A convolutional long short-term memory based neural network for epilepsy detection from EEG. IEEE Trans Instrum Meas. 2022;71:1–11.
37. Tawhid MNA, Siuly S, Wang K, Wang H. Automatic and efficient framework for identifying multiple neurological disorders from EEG signals. IEEE Trans Technology and Society. 2023;4(1):76–86.
38. Shin H-C, et al. Deep convolutional neural networks for computer-aided detection: CNN architectures, dataset characteristics, and transfer learning. IEEE Trans Med Imaging. 2016;35(5):1285–98.
39. Sharma R. Automated human emotion recognition using hybrid approach based on sensitivity analysis on residual time-frequency plane with online learning algorithm. Biomed Signal Process Control. 2023;84:104913. https://doi.org/10.1016/j.bspc.2023.104913.
40. Jelic V, Shigeta M, Julin P, Almkvist O, Winblad B, Wahlund LO. Quantitative electroencephalography in mild cognitive impairment: longitudinal changes and possible prediction of Alzheimer's disease. Neurobiol Aging. 1996;17(3):453–60.
41. Dauwels J, Vialatte F, Cichocki A. Diagnosis of Alzheimer's disease from EEG signals: where are we standing? Curr Alzheimer Res. 2010;7(6):487–505.
42. Fernández A, Hornero R, Gómez C, Turrero A, Gil-Gregorio P. Complexity analysis of spontaneous brain activity in Alzheimer disease and mild cognitive impairment: an MEG study. Alzheimer Dis Assoc Disord. 2010;24(2):182–9.
43. Claus JJ, Kwa VI, Teunisse S, Walstra GJ, van Gool WA, Koelman JH. Slowing on quantitative spectral EEG is a marker for rate of subsequent cognitive and functional decline in early Alzheimer disease. Alzheimer Dis Assoc Disord. 1998;12(3):167–74.
44. Babiloni C, Vecchio F, Lizio R, Ferri R, Rodriguez G, Marzano N, Frisoni GB, Rossini PM. Resting state cortical rhythms in mild cognitive impairment and Alzheimer's disease: electroencephalographic evidence. J Alzheimers Dis. 2011;26(s3):201–14.
45. Chen Y, Wang H, Zhang D, Zhang L, Tao L. Multi-feature fusion learning for Alzheimer's disease prediction using EEG signals in resting state. Front Neurosci. 2023;17:1272834.
46. Parihar A, Swami PD. EEG classification of Alzheimer's disease, frontotemporal dementia and control normal subjects using supervised machine learning algorithms on various EEG frequency bands. Int J Sci Technol Manag. 2023;12(6):82–9.

Terms and Conditions

Springer Nature journal content, brought to you courtesy of Springer Nature Customer Service Center GmbH (“Springer Nature”).
Springer Nature supports a reasonable amount of sharing of research papers by authors, subscribers and authorised users (“Users”), for small-scale personal, non-commercial use provided that all copyright, trade and service marks and other proprietary notices are maintained. By accessing, sharing, receiving or otherwise using the Springer Nature journal content you agree to these terms of use (“Terms”). For these purposes, Springer Nature considers academic use (by researchers and students) to be non-commercial.
These Terms are supplementary and will apply in addition to any applicable website terms and conditions, a relevant site licence or a personal subscription. These Terms will prevail over any conflict or ambiguity with regards to the relevant terms, a site licence or a personal subscription (to the extent of the conflict or ambiguity only). For Creative Commons-licensed articles, the terms of the Creative Commons license used will apply.
We collect and use personal data to provide access to the Springer Nature journal content. We may also use these personal data internally within ResearchGate and Springer Nature and as agreed share it, in an anonymised way, for purposes of tracking, analysis and reporting. We will not otherwise disclose your personal data outside the ResearchGate or the Springer Nature group of companies unless we have your permission as detailed in the Privacy Policy.
While Users may use the Springer Nature journal content for small scale, personal non-commercial use, it is important to note that Users may not:

1. use such content for the purpose of providing other users with access on a regular or large scale basis or as a means to circumvent access control;
2. use such content where to do so would be considered a criminal or statutory offence in any jurisdiction, or gives rise to civil liability, or is otherwise unlawful;
3. falsely or misleadingly imply or suggest endorsement, approval , sponsorship, or association unless explicitly agreed to by Springer Nature in writing;
4. use bots or other automated methods to access the content or redirect messages
5. override any security feature or exclusionary protocol; or
6. share the content in order to create substitute for Springer Nature products or services or a systematic database of Springer Nature journal content.

In line with the restriction against commercial use, Springer Nature does not permit the creation of a product or service that creates revenue, royalties, rent or income from our content or its inclusion as part of a paid for service or for other commercial gain. Springer Nature journal content cannot be used for inter-library loans and librarians may not upload Springer Nature journal content on a large scale into their, or any other, institutional repository.
These terms of use are reviewed regularly and may be amended at any time. Springer Nature is not obligated to publish any information or content on this website and may remove it or features or functionality at our sole discretion, at any time with or without notice. Springer Nature may revoke this licence to you at any time and remove access to any copies of the Springer Nature journal content which have been saved.
To the fullest extent permitted by law, Springer Nature makes no warranties, representations or guarantees to Users, either express or implied with respect to the Springer nature journal content and all parties disclaim and waive any implied warranties or warranties imposed by law, including merchantability or fitness for any particular purpose.
Please note that these rights do not automatically extend to content, data or other material published by Springer Nature that may be licensed from third parties.
If you would like to use or distribute our Springer Nature journal content to a wider audience or on a regular basis or in any other manner not expressly permitted by these Terms, please contact Springer Nature at

onlineservice@springernature.com